ELSEVIER

Thermochimica Acta 323 (1998) 109–121

thermochimica acta

Determination of the thermal conductivity in zirconia based inert matrix nuclear fuel by oscillating differential scanning calorimetry and laser flash

M.A. Pouchon[a,b,*], C. Degueldre[a,b], P. Tissot[b]

[a] *Paul Scherrer Institute, Laboratory for Materials Behaviour, CH-5232 Villigen PSI, Switzerland*
[b] *University of Geneva, Groupe de Chimie Appliquée, CH-1211 Geneva 4, Switzerland*

Received 20 March 1998; accepted 26 July 1998

Abstract

The performances of oscillating differential scanning calorimetry (ODSC) and laser-flash technique in determining the thermal conductivity and the specific heat of zirconia-based materials, analogous to a potential nuclear fuel, were compared. The tested materials were $(Zr_{1-x-y-z},Y_x,Er_y,Me_z)O_{2-(x+y)/2}$, with Me=Ce or Th. The measured specific heats were around 0.4 J K^{-1} g^{-1} and the thermal conductivities ranged from 2 to 3 W K^{-1} m^{-1}. The ODSC measurements resulted in c_p values. The thermal conductivity was derived from two complementary measurements, one with a thin and the other with a thick sample. The laser-flash technique directly delivered the thermal diffusivity of the sample; consequently, the specific heat capacity c_p has to be known for determining the thermal conductivity. The ODSC measurements were affected by the position of the sample on the support. This, consequently, influenced the reproducibility of the measurements. The reproducibility of the scans by laser flash was excellent. Thermal conductivity decreased with increase in the stabilizer (Y, Er) concentration. This trend was justified on the basis of a model including concentration and size of the oxygen vacancies.

Keywords: Heat conductivity; Innovative nuclear fuel; Laser flash; Oscillating differential scanning calorimetry; Zirconia-based ceramics

1. Introduction

A zirconia-based inert matrix has been suggested for burning in light-water reactor (LWR) plutonium excesses which are due to the discontinuation of nuclear military programs and to the worldwide increase in use of nuclear energy [1]. The world production of plutonium, estimated at the end of 1990, was ca. 650 tons [1,2] and Switzerland produces annually (1993) ca. 750 kg of plutonium [1,2]. The use of mixed oxide, $(U,Pu)O_2$, is not sufficient to balance this production. An efficient strategy based on the use of a U-free fuel is necessary. An inert-matrix fuel material, based on yttria-stabilised zirconia $(Zr_x,Y_y)O_{2-y/2}$ (fluorite structure) as inert component, has been studied because of its high melting point, its low neutron-capture cross section, and its low chemical reactivity and because of the possibility of recycling the cladding material of LWR's (i.e. Zircalloy) from significant waste stream.

A rare-earth oxide may be added as burnable poison component. Erbium oxide was selected by Degueldre et al. [1], while gadolinium oxide was chosen by Nitani et al. [3]. The advantage of erbium in a single-phase zirconia-based material is that it may contribute to the stability of the solid solution [4]. These inert-matrix components are selected to dissolve the

*Corresponding author. Fax: +41-56-310-2205, e-mail: pouchon@psi.ch

0040-6031/98/$ – see front matter
PII: S0040-6031(98)00504-8

actinide oxide, or in this work CeO_2 or ThO_2 taken as analogous compounds of PuO_2. The phases composed of the inert-matrix material and ThO_2 or CeO_2 are called simulated fuel.

Nevertheless, zirconia-derived materials are reported to have a rather low thermal conductivity. This is a negative aspect about energy transfer from the fuel pellet towards the coolant in the reactor. The purpose of this paper is to present the measured thermal conductivities of selected fuel analogue zirconia-based materials. The oscillating differential scanning calorimetric (ODSC) and laser-flash methods were applied. Results are compared with emphasis on the precision and accuracy of the results.

2. Methodological background

2.1. Principles of the measuring techniques

Analyses by differential scanning calorimetry (DSC) are based on the heat capacity difference of the system at two different positions. These positions are called reference and sample positions. Both sides are charged with a support device, this can be an aluminium pot with cover or a simple aluminium plate, but it is always the same device on both sides. Both sides can be charged with a sample. In the following descriptions the support–sample system is called the sample. By applying the same heating rate onto both samples, the heat capacity difference yields a temperature gradient. The two samples are connected and the temperature gradient yields a heat flow Φ (see Fig. 1(a)). In conventional DSC, the heating rate is constant. The ODSC is derived from DSC by applying a temperature modulation onto the DSC signal. It allows the application of a sufficient temperature gradient with a small signal amplitude. The analysis can, consequently, be made under almost isothermal conditions.

For the laser-flash test, an energy impulse is applied to one side of the sample. This photon energy shot must be transformed to a thermal impulse. Because the inert-matrix material is semi-transparent, a sample coating is required (e.g. gold and carbon) in order to absorb light and yield a heat impulse on the front side. Without such a surface treatment, the energy transfer would be driven by a combination of phonon and photon transport. The back side of semi-transparent samples is also coated and the heat signal is detected with the help of an infrared detector.

2.2. Theoretical background and modelling

In a nuclear fuel, a fission-product recoil yields a thermal spike of the order of 3000 K over a 10 nm range, for a period of the order of 10^{-11} s [5,6]. In a

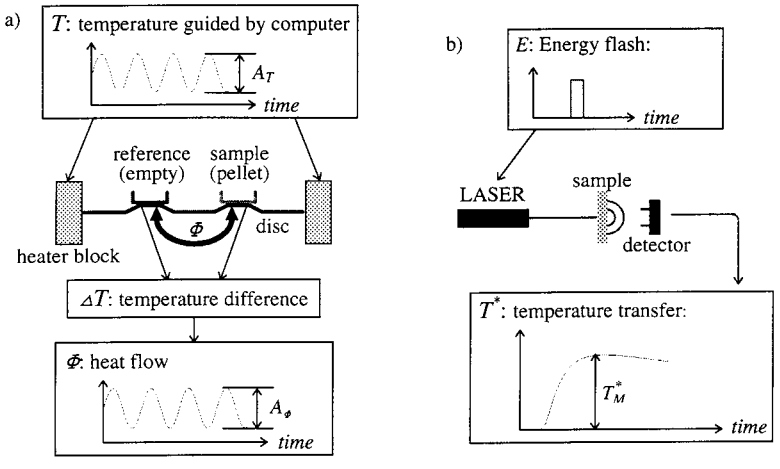

Fig. 1. Schemes explaining the principle of the two measurement techniques: (a) 'ODSC' method: A sinusoidal temperature signal is applied to the heater block of the ODSC equipment and the temperature difference between sample and reference sides is measured; and (b) 'laser-flash' method: A laser flash induces an energy pulse onto the front side of the sample, the energy is then transferred to the backside of the pellet from where it is detected by an IR detector.

semi-transparent material, this energy can be transferred by phonons and by photons. In a conservative way, this paper deals only with the phonon part of the energy transfer.

The phonon conductivity κ_0 is currently modelled on the basis of its inverse, whose variation with the temperature (T) may be modelled as,

$$\kappa_0^{-1} = A + BT \tag{1}$$

which, according to Ambegaokar [7], yields:

$$A = \frac{4\pi^2 V_0 T_D}{\overline{v}^2 h} \times \Gamma \tag{2}$$

and (e.g. Gibby [8]):

$$B = \frac{\gamma^2 h^3}{3.81\overline{M}(\overline{V}_0)^{1/3}(kT_D)^3} \tag{3}$$

$\Gamma = \Sigma\Gamma_i$ may be estimated as follows (see Ref. [9] or [8]):

$$\Gamma_i = \frac{x_i}{12}\left[\left(\frac{M_i - \overline{M}}{\overline{M}}\right)^2 + \varepsilon\left(\frac{r_i - \overline{r}}{\overline{r}}\right)^2\right] \tag{4}$$

for the materials of interest in this study, i.e. for binary, ternary or quaternary mixtures $(M_{1-x-y-z}, M'_x, M''_y, M'''_z)O_{2-u}$ with a matrix material M and the dopants M′, M″ and M‴ (e.g. for M and M‴ tetravalent and for M′ and M″ trivalent $2u = x + y$). In Eq. (4), x_{M^i} the molar fraction of the component i, M_{M^i} its mass and r_{M^i} its ionic radius, OV stands for oxygen vacancy and $x_M + \Sigma x_{M^i} + x_O + x_{OV} = 1$. ϵ is given by $32(1+1.6\gamma)^2$, where γ is the Grüneisen constant. In this equation, the average atom mass and object radius are given by:

$$\overline{M} = x_M M_M + \sum x_{M''^i} M_{M''^i} + x_O M_O \tag{5}$$

and

$$\overline{r} = x_M r_M + \sum x_{M''^i} r_{M''^i} + x_O r_O + x_{OV} r_{OV} \tag{6}$$

For phase heterogeneous mixtures, the values of the phonon conductivity become much lower than that dictated by this physical law. Its estimation, therefore, remains subject to hypotheses; it is also linked to the accuracy of the selected values of the parameters.

Recently, the thermal diffusivity of stabilised zirconia plasma-sprayed films of 0.2 to 0.8 mm thickness were investigated [10]. A dependence of the diffusivity was observed as a function of the sample thickness with variation for slim samples only. Since this effect was observed for samples smaller than 0.8 mm, it is not considered in this work because the samples here are larger than 1 mm.

2.3. ODSC theoretical background

In the ODSC, a sinusoidal temperature signal is applied to the heater block (see Fig. 1(a)) of the instrument. This temperature signal $T_b(t)$ is given by:

$$T_b(t) = T_{b_0} + qt + A_{T_b}\sin(\omega t) \tag{7}$$

where T_{b_0} (K) is the temperature of the block at time zero, q (K min^{-1}) the underlying heating rate, t (s) the time, A_{T_b} (K) the amplitude of the modulated temperature in the block, and ω (s^{-1}) the angular frequency of the modulation.

Here, the thermal properties of the materials are investigated at a defined temperature. When the temperature of interest is reached, the heating rate, q, is set to zero and it remains a pure oscillating signal. This state is studied for a sufficiently long time period to guarantee steady conditions. A_{T_b} is the amplitude of the induced temperature signal $T_b(t)$ of the heater block. A_{T_b} is small enough to assume isothermal conditions of the test. The angular frequency ω is, together with A_{T_b}, the factor which leads to a certain temperature gradient; moreover, ω must be adapted to A_{T_b} and to the sample material.

2.3.1. Determination of the heat capacity by ODSC

The temperature signal is induced symmetrically by the heater block to the disc (see Fig. 1(a)). Two thermocouples are used. One is placed at the reference, and the other at the sample position (see Fig. 1(a)). The heat flow between the heat block and these two positions is given by Newton's law [15]:

$$\frac{dQ}{dt} = K(T_{r,s} - T_b) \tag{8}$$

where Q (J) is the heat flowing between two positions (r or s and b), $T_{r,s}$ (K) the temperature at reference and sample positions, and K (J K^{-1} s^{-1}) the Newton constant.

Furthermore, the temperature of a body with a thermal heat capacity C_p is influenced by a quantity of heat Q in the following manner:

$$T = \frac{Q}{C_p} + T_0 \tag{9}$$

where T_0 (K) is the initial temperature, and C_p (J K^{-1}) the heat capacity.

Eqs. (5)–(7) lead to:

$$\frac{dQ}{dt} = K\left(qt + A_{T_b}\sin(\omega t) - \frac{Q}{C_p}\right) \tag{10}$$

Solving this differential equation under isothermal conditions and then simplifying the solution leads to the following simple equation:

$$C_s - C_r = \frac{A_\Phi}{A_T}\sqrt{\frac{K^2}{\omega^2} + C_r^2} \tag{11}$$

where C_r (J K^{-1}) is the heat capacity of the reference side, C_s (J K^{-1}) the heat capacity of the sample side, A_Φ (K) the amplitude of the ODSC signal and A_T (K) the amplitude of the temperature signal. (Here, the amplitude of the temperature signal is observed at the reference position.)

2.3.2. Determination of the thermal conductivity by ODSC

To determine the thermal conductivity of a sample, an additional measurement is necessary. For the determination of the specific heat, the sample was cut to a thin disc to avoid any conductivity effects. Consequently, the sample must be some kind of rod to affect any conduction. When a periodic temperature variation is induced to one end of a rod, the temperature distribution along the rod is given by [16]:

$$T(x,t) = T(x)e^{i\omega t} \tag{12}$$

$$T(x) = a \cdot e^{-x\sqrt{\frac{i\omega}{\alpha}}} + b \cdot e^{x\sqrt{\frac{i\omega}{\alpha}}} \tag{13}$$

where α (m^2 s^{-1}) is the diffusivity constant of the rod, x (m) the axis along the rod, a, b (K) constants given by the boundary conditions

The heat flux across the end of the rod is assumed to be zero. This gives rise to the condition: $(dT/dx)_{x=L}=0$, where L is the length of the rod. The other end of the rod (base) just follows the temperature of the induced signal. Consequently, the temperature amplitude $A_T(0)$ is equal to the temperature amplitude at the sample position A_{T_s} : $A_T(0) = A_{T_s}$.

From the boundary conditions, we find:

$$b = A_T - a$$

$$a = \frac{A_T}{e^{-2L\sqrt{i\cdot\omega/\alpha}} + 1} \tag{14}$$

The heat flow through the base of the rod is given by:

$$\left(\frac{dQ}{dt}\right)_{x=0} = -\kappa_\eta S\left(\frac{dT}{dx}\right)_{x=0} \tag{15}$$

where κ_η (W K^{-1} m^{-1}) is the thermal conductivity of the rod, S (m^2) the cross-sectional area of the rod and η the porosity of the sample.

Inserting Eqs. (13) and (14) in Eq. (15) and multiplying the result by its complex conjugate yields the amplitude of the heat flow:

$$\left|\frac{dQ}{dt}\right|^2 = (\kappa_\eta T_0 S)^2 \frac{\omega}{\alpha} \times \frac{1 - 2e^{-L\sqrt{2\frac{\omega}{\alpha}}}\cos\left(L\sqrt{2\frac{\omega}{\alpha}}\right) + e^{-2L\sqrt{2\frac{\omega}{\alpha}}}}{1 + 2e^{-L\sqrt{2\frac{\omega}{\alpha}}}\cos\left(L\sqrt{2\frac{\omega}{\alpha}}\right) + e^{-2L\sqrt{2\frac{\omega}{\alpha}}}} \tag{16}$$

furthermore:

$$A_\Delta = \left|\frac{dQ}{dt}\right| = T_0\omega C_P' \tag{17}$$

where κ_η (W K^{-1} m^{-1}) is thermal conductivity of the sample, A_Δ (W s^{-1}) the heat flow amplitude and C_P' (W K^{-1}) the apparent heat capacity.

Let us assume that:

$$L\sqrt{2\frac{\omega}{\alpha}} \gg 0 \tag{18}$$

The thermal conductivity of the sample κ_η is then given by:

$$\kappa_\eta = \frac{A_\Phi^2}{\omega\rho_\eta C_P T_0^2 S^2} \equiv \frac{\omega C_P'}{\rho C_P A^2} \tag{19}$$

where ρ_η (kg m^{-3}) is the sample density.

Heat losses at the surface of the sample lead to an error. This error can be approximately determined by measuring a reference material with similar dimensions and heat conductivity values. This yields a correction term, which is given by (the calculations can again be found in Ref. [16]):

$$R = \sqrt{\kappa_\eta\kappa_M} - \kappa_\eta \tag{20}$$

where R (W m^{-1} K^{-1}) is the correction term, κ_M (W m^{-1} K^{-1}) the apparent thermal conductivity and κ_η (W m^{-1} K^{-1}) the thermal conductivity of the sample.

The measurement of a sample with an unknown thermal conductivity will then be corrected using the following equation:

$$k_\eta = \frac{\kappa_M - 2R + \sqrt{\kappa_M^2 - 4R\kappa_M}}{2} \quad (21)$$

2.4. Laser flash

The phonon or thermal conductivity is derived from the experimental thermal diffusivity. It may be obtained by using the equation:

$$\kappa_\eta = \alpha c_p \rho_\eta \quad (22)$$

where κ_η (W m^{-1} K^{-1}) is the thermal conductivity, α (m^2 s^{-1}) the thermal diffusivity of the sample, c_p (J kg^{-1} K^{-1}) the specific heat capacity and ρ_η (kg m^{-3}) the sample density.

The thermal diffusivity is derived from the thermogram recorded. (The scan can be studied in Fig. 1(b) in the Section 2.1.) It is obtained from the temperature variation measured on the back side of the sample. The interpretation is derived from the method described in Ref. [11]; it leads to the formula:

$$\ln(T^*\sqrt{t}) = \ln\left(\frac{2T_M^* d}{\sqrt{\pi\alpha}}\right) - \frac{L^2}{4\alpha t} \quad (23)$$

where L (m) is the thickness of the sample, t (s) the time after laser pulse, T^* (K) the transferred temperature difference at time t and T_M^* (K) the maximal temperature difference transfer.

2.5. Porosity correction of the conductivity

The investigated pellets had porosities from 6 to 20% (see Table 4 in Section 3.1). The thermal conductivities of the porous samples are corrected to obtain the conductivity values of the solid materials. The correction equation used is:

$$\kappa_0 = \kappa_\eta(1-\eta)^{-1.7} \equiv \kappa_\eta(\rho_\eta^{-1}\rho_0)^{1.7} \quad (24)$$

where κ_0 (W m^{-1} K^{-1}) is the thermal conductivity of the solid material, κ_η (W m^{-1} K^{-1}) the thermal conductivity of the porous sample, η the porosity of the sample, $\rho_\eta\rho_0^{-1}$ the relative density of the sample and ρ_0 (kg m^{-3}) the theoretical density of the material.

This formula can be found in [12]. An overview of the correction models is given in Appendix A.

3. Experimental

3.1. Material preparation and analyses

The preparation of all zirconia-based materials was carried out by the wet route, because it was earlier found that it yields the large material density [13] required for the test. All solutions were prepared by mixing nitrate solution of each element (Zr, Y, Er, Th or Ce) composing the final product. Co-precipitation was carried out by adding ammonia under strong stirring. The precipitate was filtered on a paper filter and washed 10 times with ultrapure water. The filtered phase was contacted with alcohol and milled, utilising a Retch unit with zirconia container and bowls. The wet powder was then dried 24 h at 420 K. The dried powder was then manually desegregated prior to calcination for 5 h at 900 K. The calcinated powder was milled again, utilising the Retch unit with zirconia vessel. The final powder was then pressed, two different brands of pellets were produced, one 5 mm in diameter and the other 11 mm in diameter. The 5 mm pellets were pressed with 700 MPa for 1 min and the 11 mm pellets with 352 MPa for 10 s. Pelletised samples were then sintered in an oven with a temperature programme including a first step at 1475 K for 4 h followed by a final step of 48 h at 1875 K.

The sintered pellets were ca. 10 or 5 mm in diameter. The 10 mm pellets were cut to approximately 1 mm thickness (L) and the 5 mm pellets were cut to two different dimensions, namely 1 mm and 5 mm thickness (L). The cutting was performed by a diamond saw. Table 2 indicates the masses of the pellets 5 mm in diameter and 1 mm in height. These were used to measure the heat capacity of the different compositions. The density of the pellets used for the conductivity measurement was determined by measuring the sizes (diameter and thickness) and weight utilising a Mettler balance (AG204). Size (L), mass (m) and densities (ρ_η and $\rho_\eta\rho_0^{-1} \times 100$) are given in Table 4. ρ_0 is the theoretical density and ρ_η the geometrical density of the pellet. The relative densities varied from 80 to 94%. For each composition, there were three different pellets which are described in Appendix B.

The theoretical density was calculated from a simple approach based on the macroscopic density of each component. X-ray diffraction (XRD) analysis was carried out on a crushed pellet of the fabrication batch

to identify the phases and to determine the lattice parameter. The XRD unit was a Phillips diffractometer PW1710, equipped with a Cu X-ray tube. The samples were analysed after crushing and lattice parameters were measured with a precision better than ± 0.01 Å. Prior to measurement of thermal conductivity, the samples were examined by X-ray diffraction to identify the phases and to confirm the absence of any other phases as the cubic phase in the inert matrix and simulated fuel materials.

3.2. Laser flash

The samples were measured by the laser-flash method at JAERI, Japan [14]. Disc samples of 10 mm in diameter and ca. 1 mm in thickness were subjected to a preliminary examination, and those presenting any heterogeneity, small fissure or hole were discarded. Since the samples were white or slightly coloured, the surface of the disc samples was coated with gold and carbon. Gold was vapour deposited on the surface to allow good thermal contact onto the semi-transparent material. Surface treatment was completed by carbon powder spray on the surface to efficiently absorb the laser beam. The coating was very thin so that its influence on the measured thermal diffusivity was <1%. The measurements were performed in vacuum below 3×10^{-3} Pa.

The sample was heated in an electric furnace to the required temperatures and the sample temperature was measured with an IR detector. The method consists of illuminating the front face of the disc with a short laser pulse, creating at the surface a heat pulse when the light is adsorbed. The energy of the laser pulse was 6 J, which allows locally a temperature increase of the sample surface of ca. 10 K. The thermal diffusivity, α, is deduced from the thermal transient of the rear face, called the thermogram. The temperature rise at the rear surface was measured by an In–Sb infrared detector, after the front surface of the sample was heated by a ruby laser pulse. The data of the temperature change were analysed using a logarithmic method [14].

3.3. Oscillating differential scanning calorimetry (ODSC)

At the University of Geneva, a Seiko 220 DSC unit was adapted for ODSC measurements. This unit was already equipped with a programmer for sinusoidal temperature variation. The output signal was recorded as a raw data set and must be evaluated using an separate computer unit with the calculation method given by Wunderlich [15]. Sapphire was used for calibration and glass with a well-known heat capacity was measured to control the reliability of the equipment. The parameters used for the ODSC measurement were the following. The explanation of the different parameters can be found in the Section 2.3.

t_{tot} total measuring time; around 30 min
A_{T_b} 0.5 K
ω $2.0\pi\times10^{-2}$ s^{-1}

At room temperature the natural cooling of the unit block is slow. Therefore, a fast sinusoidal temperature signal cannot be obtained without additional cooling. The ODSC cell was consequently cooled by liquid nitrogen.

Disc samples of 5 mm diameter and 1 mm thickness were used for the c_P measurements. The samples were placed into an aluminium pot with cover. The sample-containing pot–cover unit was tightened by a manual press to ensure a good thermal contact of the unit. The prepared samples were positioned manually on the sample holder.

A TA-Instruments 2920 unit was also used, courtesy Du Pont de Nemours. This unit was originally equipped with the ODSC option and no additional programming was required. The parameters have been set to the following values:

t_{tot} total measuring time; around 30 min
A_{T_b} 1 K
ω $2.5\pi\times10^{-2}$ s^{-1}

The heat capacity measurements on the samples already measured were repeated with the TA-Instruments equipment. Further, heat conductivity measurements were performed. Cylindrical pellets with 5 mm diameter and 5 mm height were set on an aluminium plate using a heat-conducting paste. This unit was then placed on the sample holder again.

For the thermal-loss correction, glass with a known thermal conductivity was tested. This reference sample had dimensions similar to the other pellets and its thermal conductivity was also in a similar range.

4. Results and discussion

4.1. Heat capacity

The heat capacity of the materials must first be obtained to calculate the thermal conductivity using Eq. (19). Therefore, an oscillating temperature must be applied to the equipment. An ODSC signal is, consequently, measured as output. With the amplitudes of these two signals, the heat capacity can be calculated using Eq. (11). However, if the heat capacity is already known, the Newton constant, K, of the instrument may be calculated.

Figs. 2 and 3 illustrate the ODSC measurement with the simulated fuel material $(Zr_{0.70},Y_{0.15},Er_{0.05},Ce_{0.10})O_{1.9}$. Fig. 2(a) shows the temperature programme induced by the Seiko instrument used for the measurement of the simulated fuel mentioned before. Fig. 2(b) shows a magnification of the average temperature signal. The average is taken over one period. A deviation from linearity means a difference from a pure sinusoidal signal of the original data. Fig. 2(c) shows the amplitude of the signal. The resulting ODSC signal is presented in Fig. 3(a). Again, a magnification of the average is displayed in Fig. 3(b).

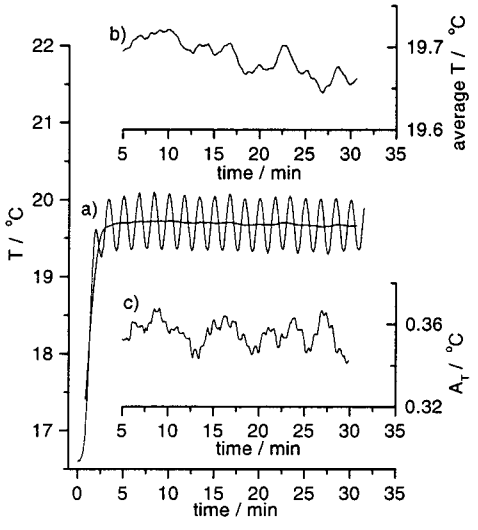

Fig. 2. Temperature signal applied to the heater block. (a) Temperature signal; (b) average temperature (average over one period); and (c) signal amplitude.

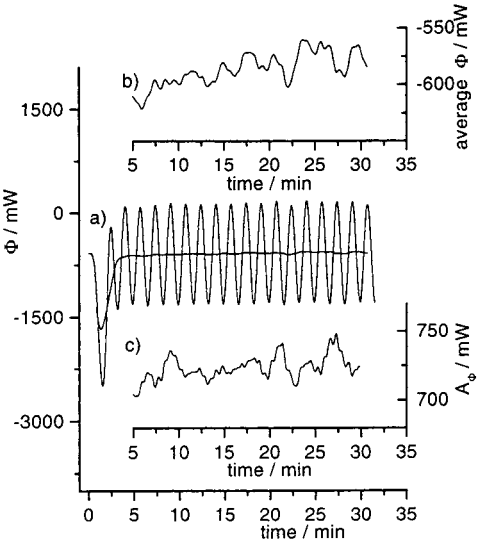

Fig. 3. ODSC signal measured between reference and sample position. (a) ODSC signal; (b) average ODSC signal (average over one period); and (c) signal amplitude.

Division of the amplitudes A_Δ (Fig. 3(c)) and A_T (Fig. 2(c)) gives the required information about the heat capacity (see Eq. (11)). Therefore, the average value of a representative data area is taken (see Fig. 4).

Fig. 5(a and b) illustrate the heat capacity measured with both equipments; with the Seiko as well as the TA-Instruments machine. With both apparatuses the specific heat capacity was detected by ODSC.

4.2. Thermal conductivity

The conductivities were measured using two techniques, namely laser flash and ODSC. Table 1 gives the conductivity values for all studied compositions obtained without porosity correction.

Fig. 6(a and b) shows the porosity corrected thermal conductivities for the various material compositions (for porosity correction see Section 2.5 and Appendix A).

On increasing the concentration of dopants the thermal conductivity shows a decreasingly trend. The temperature independent term A in Eq. (1) is coupled linearly to the scattering cross-section parameter Γ (see Eq. (2)). Γ_i, the ith part of Γ, is given in Eq. (2). A large differences between the mass M_i and the average mass of the system $\overline{M}$ yields an enlargement of the $x_i(M_i - \overline{M})\overline{M}^{-1}$ term (see Eq. (4)). Simi-

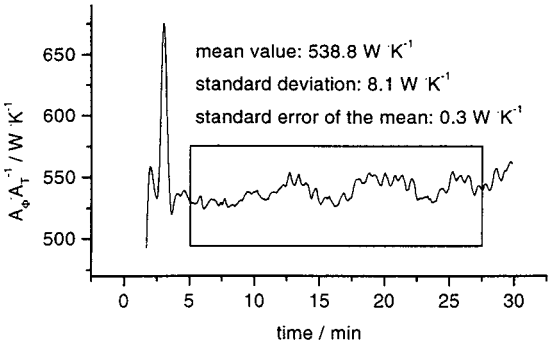

Fig. 4. Statistics of $A_{\Phi}A_{T}^{-1}$ ratio used for the calculation of the c_P values. This statistical investigation only illustrates the stability concerning one measurement. The statistics on the calculated c_P values can be found in Appendix C.

Table 1
Uncorrected thermal conductivities of the studied samples at RT, measured by laser flash and by ODSC

Sample	κ_{η}/W m^{-1} K^{-1}	
	laser	ODSC
Zr	1.99	2.30
Zr10Y	1.93	1.80
Zr20Y	1.30	2.01
Zr30Y	1.46	1.78
Zr10Er	1.55	2.02
Zr10Y5Er	1.73	1.69
Zr20Y5Er	1.59	1.53
Zr15Y5Er10Ce	1.59	1.74
Zr15Y5Er10Th	1.10	1.42
Zr10Y7Er15Ce	1.46	1.07

larly, a large difference in the ionic radius r_i and the average ionic radius $\overline{r}$ yields an enlargement of the term $x_i(r_i - \overline{r})\overline{r}^{-1}$ (see Eq. (4)). Consequently, important differences exist in the different dopant ionic radii and molar mass increase Γ and the resistivity. The conductivity as an inverse of the resistivity decreases. This justifies the experimental results shown in the Fig. 6(a and b). Full modelling is, however, limited by the structural changes from ZrO_2 (monoclinic) to $(Zr_{1-x-y-z},Y_x,Er_y,Ce_z)O_{2-(x+y)/2}$ (fluorite cubic).

5. Concluding remarks

Thermal conductivity measurements of zirconia-based inert-matrix fuel have been achieved by the oscillating differential scanning calorimetry and laser-flash technique. Comparable results were obtained. A

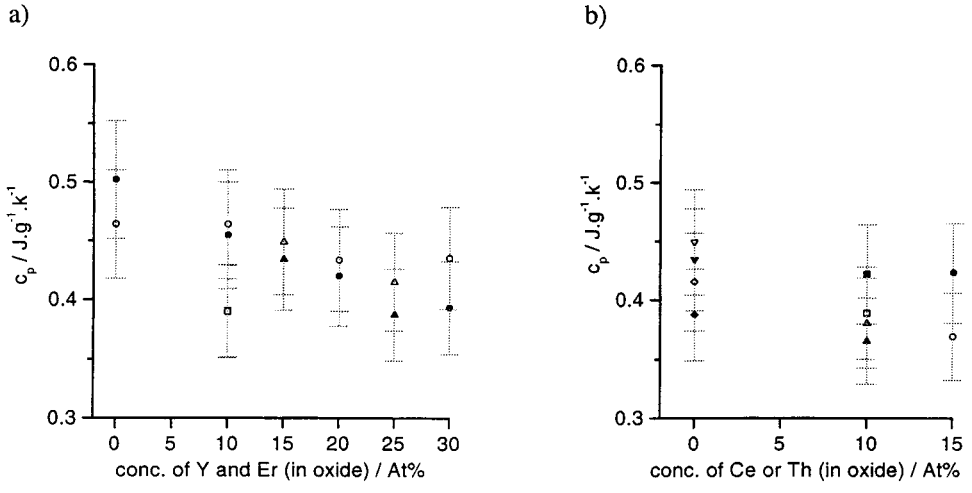

Fig. 5. Heat capacity of zirconia-based materials measured with two different ODSC instruments, with *solid symbols*: Seiko at 47°C and *open symbols*: TA-Instr. at 20°C: (a): Ternary systems: $(Zr_{1-x-y},Y_x,Er_y)O_{2-(x+y)/2}$ with an erbia part of (At%): (●) 0; (■) 5; and (▲) 10. (b): Quaternary systems: $(Zr_{1-x-y-z},Y_x,Er_y,Ce_z)O_{2-(x+y)/2}$ and $(Zr_{1-x-y-z},Y_x,Er_y,Th_z)O_{2-(x+y)/2}$. The different material compositions were: (▼) $(Zr_{0.70},Y_{0.10},Er_{0.05})O_{1.925}$; (◆) $(Zr_{0.70},Y_{0.20},Er_{0.05})O_{1.875}$; (▲): $(Zr_{0.70},Y_{0.15},Er_{0.05},Ce_{0.10})O_{1.900}$; (■) $(Zr_{0.70},Y_{0.15},Er_{0.05},Th_{0.10})O_{1.900}$; and (●) $(Zr_{.68},Y_{.1},Er_{.07},Ce_{.15})O_{1.915}$.

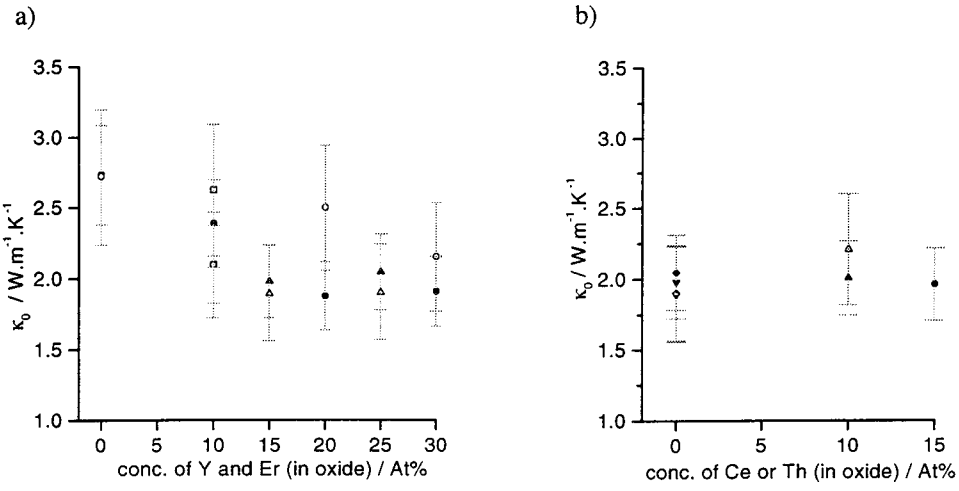

Fig. 6. Thermal conductivity of zirconia based materials at 20°C measured by the two studied techniques, *solid symbols*: laser flash, *open symbols*: ODSC. (a): Ternary systems: $(Zr_{1-x-y},Y_x,Er_y)O_{2-(x+y)/2}$ with an erbia part of (At%): (●) 0, (■) 5; (▲) 10. (b): Quaternary systems: $(Zr_{1-x-y-z},Y_x,Er_y,Ce_z)O_{2-(x+y)/2}$. The different material compositions were: (▼) $(Zr_{0.70},Y_{0.10},Er_{0.05})O_{1.925}$; (◆) $(Zr_{0.70},Y_{0.20},Er_{0.05})O_{1.875}$; (▲) $(Zr_{0.70},Y_{0.15},Er_{0.05},Ce_{0.10})O_{1.900}$; and (●) $(Zr_{0.68},Y_{0.1},Er_{0.07},Ce_{0.15})O_{1.915}$.

systematic study was carried out for $(Zr_{1-x-y-z},Y_x,Er_y,Me_z)O_{2-(x+y)/2}$ with Me=Ce or Th. The thermal conductivity decreases from 3 to 2 W m^{-1} K^{-1} when the dopant (Y, Er) concentration increases up to 30 At%. This trend is justified by the theory based on the properties of the oxygen vacancies in the cubic lattice generated by the addition of dopant.

Acknowledgements

Thanks are due to Mrs. H. Lartigue and Mr. A. Desponds for their measurements by ODSC at the University of Geneva and Du Pont de Nemours technical centre, Geneva. The technical assistance of Mr. M. Takano is acknowledged for laser-flash tests at JAERI. P. Heimgartner and T. Graber are thanked for their technical support. G. Ledergerber, head of the fuel section, is thanked for useful and constructive discussions about this work.

Appendix A: Porosity corrections

Several equations have been proposed in order to correct the thermal κ_η conductivity of solid solutions with regard to porosity η. Four corrections derived from theoretical models and three empirical formula are presented here.

- The simple linear correction, which physically supposes tube-shaped pores whose axes are parallel to the temperature gradient:

$$\kappa_\eta = \kappa_0(1-\eta) \tag{A.1}$$

- The correction derived from a model supposing closed spherical pores [17]:

$$\kappa_\eta = \kappa_0(1-\eta)^{1.5} \tag{A.2}$$

- A model handling open porosity yields [17]:

$$(1-\eta)(\kappa_0-\kappa_\eta)\left[2\frac{1-\cos^2\psi}{\kappa_0-\kappa_\eta}+\frac{\cos^2\psi}{\kappa_\eta}\right] = \eta(2-\cos^2\psi) \tag{A.3}$$

  where ψ is the orientation angle of the ellipsoidal pores with respect to the heat gradient.
- Porosity correction for UO_2 by determining the structure of the pores and calculation by finite-element method yields [12]:

$$\kappa_\eta = \kappa_0(1-\eta)^{1.7\pm0.2} \tag{A.4}$$

- A modified Loeb formula is suggested, based on measurements on unirradiated UO_2 fuel [18,19]:

$$\kappa_\eta = \kappa_0(1 - \xi\eta) \quad \text{(A.5)}$$

where η is an empirical parameter.

- Another empirical correction proposed is the Maxwell–Eucken equation [20]:

$$\kappa_\eta = \kappa_0 \frac{1-\eta}{1+\beta\eta} \quad \text{(A.6)}$$

where β is an empirical parameter.

- The Loeb and the Maxwell–Euken equations can be replaced with [21]:

$$\kappa_\eta = \kappa_0(1-\eta)^{2.5} \quad \text{(A.7)}$$

The following figure shows a plot of the correction in the porosity range from 0 to 30%. Parameters are indicated in the legend.

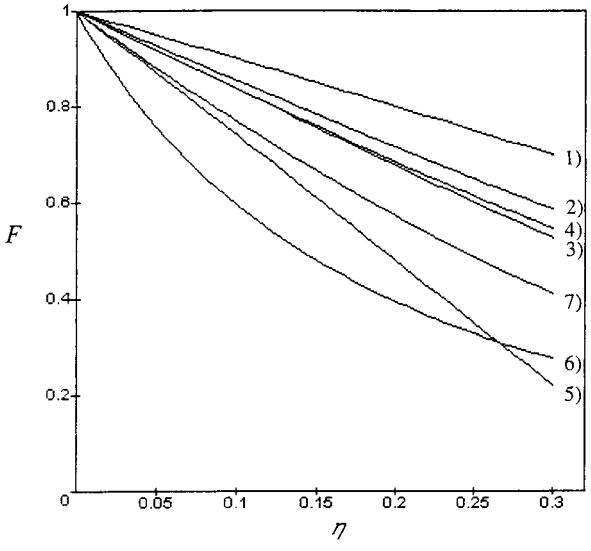

Figure. Correction factor F as a function of the porosity η. The numbers on the right-hand side of the graphs indicate the correction functions namely: (1) simple linear correction; (2) correction with spherical pores; (3) correction with open porosity with randomly distributed pores angles ($\cos^2\psi$=1/3); (4) correction based on finite-element calculus for a UO_2 material. The graph just shows the curve calculated with the intermediate exponent value 1.7 (without the range ±0.2); (5) empirical correction (modified Loeb), with ξ=2.6–0.5×10^{-5}T (T=20, temperature in °C) [20]; (6) Maxwell–Euken correction, with β=6.5–0.00469T (T=291, temperature in K) [21]; and (7) correction derived from points (5) and (6).

In this work, the correction (Eq. (A.4)) by the finite-element method was selected. It yielded corrected conductivities between the values of the two theoretical models (Eqs. (A.2) and (A.3)) which are more general than the empirical formulas (Eqs. (A.5)–(A.7)). These empirical equations are derived from data of UO_2 samples.

Appendix B: Sample data

Tables 2–4

Appendix C: Error calculation

C.1. Data from literature

The c_P measurements by ODSD are calibrated using a sapphire standard sample. The c_P value of sapphire is taken from Touloukian [22] and its error is 0.2%.

C.2. Oscillating differential scanning calorimetry (ODSC)

C.2.1. Heat capacity

The thermal conductivity was investigated with both the equipments. For both of them a statistical determination of the error was performed:

TA-Instruments: A series of nine calibration measurements (determining of the Newton constant K, see Section 2.3) with sapphire as standard was fulfilled.

Table 2
Characterisation of samples O_t produced for the heat capacity measurements by ODSC: mass of the pellets and the measured heat capacities, once at 20°C investigated by the TA-Instr. equipment, and once at 47°C measured with the Seiko machine

Sample	m (10^{-5} kg)	$c_P^{(TA\text{-}Instr\text{-}20)}$ (J kg^{-1} K^{-1})	$c_P^{(Seiko\text{-}47)}$ (J kg^{-1} K^{-1})
Zr_O_t	4.40	0.464	0.502
Zr10Y_O_t	4.12	0.464	0.454
Zr20Y_O_t	6.63	0.435	0.393
Zr30Y_O_t	7.64	0.434	0.420
Zr10Er_O_t	6.53	0.390	0.391
Zr10Y5Er_O_t	6.63	0.449	0.434
Zr20Y5Er_O_t	8.16	0.415	0.388
Zr15Y5Er10Ce_O_t	8.42	0.381	0.365
Zr15Y5Er10Th_O_t	6.74	0.389	0.422
Zr10Y7Er15Ce_O_t	8.49	0.369	0.423

Table 3
Characterisation of samples O_T produced for the thermal conductivity measurements by ODSC: thickness, weight, density, relative density and the measured thermal conductivities of the porous and theoretically dense pellets. The equation applied for porosity correction can be found in the Section 2.5 (Diameters can be calculated from thickness (L), mass (m) and the density (ρ_η); the theoretical densities (ρ_0) can be calculated from ρ_η and $\rho_\eta\rho_0^{-1} \times 100$

Sample	L (10^{-4} m)	m (10^{-5} kg)	ρ_η (10^{-3} kg m^{-3})	$\rho_\eta\rho_0^{-1}$ 100%	κ_η (W m^{-1} K^{-1})	κ_0 (W m^{-1} K^{-1})
Zr_O_T	49.5	52.7	5.34	91	2.30	2.70
Zr10Y_O_T	51.0	51.9	5.31	91	1.80	2.11
Zr20Y_O_T	49.8	55.9	5.02	88	2.01	2.50
Zr30Y_O_T	51.1	55.5	5.02	89	1.78	2.17
Zr10Er_O_T	50.8	60.0	5.30	86	2.02	2.61
Zr10Y5Er_O_T	51.5	58.4	5.56	94	1.69	1.88
Zr20Y5Er_O_T	52.2	59.9	5.15	88	1.53	1.90
Zr15Y5Er10Ce_O_T	53.0	58.7	5.24	87	1.74	2.20
Zr15Y5Er10Th_O_T	49.4	56.6	5.00	80	1.42	2.08
Zr10Y7Er15Ce_O_T	53.0	58.7	5.39	87	1.07	1.36

Table 4
Characterisation of samples O_L produced for the thermal conductivity measurements by laser flash: thickness, weight, density, relative density and the measured thermal conductivities of the porous and theoretically dense pellets. The equation applied for porosity correction can be found in the Section 2.5 (Diameters can be calculated from thickness (L), mass (m) and the density (ρ_η) the theoretical densities (ρ_0) can be calculated from ρ_η and $\rho_\eta\rho_0^{-1} \times 100$)

Sample	L (10^{-4} m)	m (10^{-5} kg)	ρ_η (10^{-3} kg m^{-3})	$\rho_\eta\rho_0^{-1}$ 100%	κ_η (W m^{-1} K^{-1})	κ_0 (W m^{-1} K^{-1})
Zr_O_L	8.5	28.6	5.89	83	1.99	2.72
Zr10Y_O_L	8.4	30.2	5.80	88	1.93	2.39
Zr20Y_O_L	7.8	27.2	5.70	81	1.30	1.87
Zr30Y_O_L	8.3	29.7	5.61	85	1.46	1.91
Zr10Er_O_L	8.5	32.5	6.18	83	1.55	2.10
Zr10Y5Er_O_L	8.3	32.3	5.94	92	1.73	1.97
Zr20Y5Er_O_L	8.5	32.6	5.85	86	1.59	2.05
Zr15Y5Er10Ce_O_L	8.2	31.2	6.03	87	1.59	1.93
Zr15Y5Er10Th_O_L	8.3	32.2	6.23	80	1.10	1.60
Zr10Y7Er15Ce_O_L	8.6	30.1	6.20	84	1.46	1.97

The setup of the unit was maintained (for the setup, see Section 3.3) and the standard was repositioned for every measurement. A variation of 4.0% [23] was found. The error from the literature value for the sapphire heat capacity of 0.2% and a measurement error for the mass of 0.1% were added to this statistical error, resulting in a total error for the calibration of 4.3%. For determining the heat capacity, a second similar measurement with the investigated material was necessary. The statistical error was also assumed to be 4.0% (same procedure) and again an error of 0.1% for the mass is added resulting in 4.1% error for a sample measurement. In Eq. (11), these two errors sum up to 8.4%.

Seiko: Again a series of calibration measurements was performed. The setup was also maintained (see Section 3.3) and for every four measurements a placement and taking off procedure was fulfilled. This resulted in a variation of 2.3%. Again the same literature and the mass error, as before, were added to this statistical error resulting in 2.6% total error for the calibration. With the same calculation as above this would result in an error of the heat capacity of 5.0% for a sample.

These errors were checked by selecting two materials and making a statistical investigation about their final c_P value. For ZrO_2, three measured c_P values at 20°C were taken into account. One from the TA-

Instruments equipment and two from the Seiko machine. The mean value of these measurements was 0.446 J g^{-1} K^{-1} and the standard deviation was 0.018 J g^{-1} K^{-1}, which is 4.1% of the mean value. The literature value for this material at 20°C is 0.450 J g^{-1} K^{-1}. For the quaternary material $(Zr_{0.80}Y_{0.15}Er_{0.50}Ce_{0.10})O_{1.9}$, again three different c_P measurements at 20°C were calculated. One measured by the TA-Instrument and two by the Seiko unit. The mean value was 0.386 J g^{-1} K^{-1} and the standard deviation 0.006 J g^{-1} K^{-1}, which is 1.49% of the mean value.

C.2.2. Thermal conductivity

The thermal conductivity was investigated with the TA-Instrument unit. To calculate the thermal conductivity, both C_P and apparent C_P (called C'_P) values were needed. The same Newton constant was taken for determining both of them. The total error can be derived from Eq. (19). It is the sum of the relative errors for $C'_P 2/C_P$, the angular frequency ω, twice the cross section S and the porous sample density ρ_η.

The error on $C'_P 2/C_P$ is 16.2%. The statistical error of three single ODSC measurements and one calibration error are added. Presently, C_P and C'_P are calculated using the same Newton constant; therefore, the calibration error (error of Newton constant) cancels in the ratio value C'_P/C_P. Eq. (19) includes the heat capacities, hence the error on the mass measurement is ignored. The error of the angular frequency is negligible. $\Delta S/S$ is 0.4% supposing a $\pm 10^{-5}$ m precision for a 5 mm pellet. $\Delta\rho_\eta/\rho_\eta$ is 0.7%, supposing the same cross-sectional error plus an error of 0.2% for the height ($\pm 10^{-5}$ m precision on a pellet height of 5 mm) and an error of 0.1% for the mass. So the total error for the thermal conductivity is 17.7%.

C.3. Laser flash

For the diffusivity calculation, Eq. (23) was used. However, several calculation methods may be used to calculate the diffusivity. For simplicity the formula proposed by Parker:

$$\alpha = \frac{\text{const} \cdot L^2}{t_{1/2}}$$

where $t_{1/2}$ (s) is half of the time required for the transferred temperature to reach its maximal value and const a known constant=0.13878 was used for the calculation of error.

The *const* is well known, and its error is negligible. The thickness L of the sample is measured with a precision of $\pm 10^{-5}$ m and L ranges between 0.78 and 0.86 mm. The maximal error is $\Delta L/L$=1.3%. The time detection is precise, its error is estimated to 3‰. It results in a total error of 2.9% for the diffusivity. For calculating the thermal conductivity, Eq. (22) is used. Therefrom, $\Delta\rho_\eta/\rho_\eta$ and $\Delta c_P/c_P$ must also be considered. $\Delta\rho_\eta/\rho_\eta$ is 2‰ for the cross section ($\pm 10^{-5}$ m precision for a 1-cm pellet) plus 1.3% for the height plus 0.4‰ for the measured weight. $\Delta c_P/c_P$ is 8.4%. Hence, the total error of the thermal conductivity measured by laser flash is 12.9%. (When using the ODSC-measured heat conductivity, however, using literature data precision should be better, but the accuracy is doubtful. The heat conductivity of the different compositions cannot be found in literature, a calculation using the heat conductivity of every fraction must be performed. Such a calculation does not consider phase changes.)

References

[1] C. Degueldre, U. Kasemeyer, F. Botta, G. Ledergerber, Mat. Res. Soc. Symp. Proc. 412 (1996) 15.
[2] D. Albright, F. Berkhout, W. Walker, Oxford University Press, Oxford, 1993.
[3] N. Nitani, H. Akie, H. Takano, T. Ohmichi, T. Muromura, Proc. PSI Workshop on Advanced Fuel Cycles, PSI, Villigen, Switzerland, 1995, p. 118.
[4] H. Yokokawa, N. Sakai, T. Kawada, M. Dokiya, J. Austral. Ceram. Soc. 28(1) (1992) 1.
[5] K. Izui, J. Phys. Soc. Jap. 20(6) (1965) 67.
[6] M. Waligorski, R. Hamm, R. Katz, Nucl. Tracks Radiat. Meas. 11 (1986) 309.
[7] V. Ambegaokar, Phys. Rev. 114 (1959) 488.
[8] R. Gibby, J. Nucl. Mater. 38 (1971) 163.
[9] B. Abeles, Phys. Rev. 131 (1963) 1906.
[10] A. Rudajevová, Thin Solid Films 223 (1993) 248.
[11] T. Lechner, Bestimmung der Temperaturleitfähigkeit semitransparenter Materialien mit dem Laser-impulsverfahren. Messungen an kristallinem und gesintertem Al_2O_3 und MgO, Fortschritt-Bericht, Reihe 19, Nr. 90, VDI Verlag GmbH Düsseldorf, Germany, 1996.
[12] K. Bakker, H. Kwast, E.H.P. Cordfunke, J. Nucl. Mater. 226 (1995) 128.
[13] C. Degueldre, P. Heimgartner, G. Ledergerber, N. Sasajima, K. Hojou, T. Muromura, L. Wang, W. Gong, R. Ewing, Mat. Res. Soc. Symp. Proc. 439 (1997) 625.

[14] H. James, J. Appl. Phys. 51 (1980) 4666.
[15] B. Wunderlich, Y. Jin, A. Boller, Thermochim. Acta 238 (1994) 277.
[16] Sanford M. Marcus, Wilmington, Del.; Reading Michael, London Engl. ''Method and apparatus for thermal conductivity measurements'', US Patent Number: 5,335,993 (1994).
[17] B. Schulz, High Temp. – High Press. 13 (1981) 649.
[18] A.B.G. Washington, UKAEA Report TRG Report 2236 (D) (1973).
[19] R. Brandt, G. Neuer, J. Non-Equilib. Thermodyn. 1 (1976) 3.
[20] J.K. Horhorst (Ed.), SCADAP/RELAP5/MOD2 Code Manual Vol. 4: MATPRO – a library of materials properties for light-water-reactor accident analysis, EG&G Idaho Report NUREG/CR-5273 (1990).
[21] J.H. Harding, D.G. Martin, P.E. Potter, Thermophysical and thermochemical properties of fast reactor materials, Commission of the European Communities Report EUR 12402 EN (1989).
[22] Y.S. Touloukian, Thermophysical Properties of Matter, IFI/Plenum New York-Washington, 1970.
[23] A. Desponds, technical Report: Du Pont De Nemours International S.A. Meyrin Genève, 1997.